A Modified Meshless Local Petrov–Galerkin Applied to Electromagnetic Axisymmetric Problems

Ramon D. Soares[1], Fernando J. S. Moreira[2], Renato C. Mesquita[3], David A. Lowther[4], and Naisses Z. Lima[1]

[1]Graduate Program in Electrical Engineering, Federal University of Minas Gerais, Belo Horizonte, Brazil
[2]Department of Electronics Engineering, Federal University of Minas Gerais, Belo Horizonte, Brazil
[3]Department of Electrical Engineering, Federal University of Minas Gerais, Belo Horizonte, Brazil
[4]Department of Electrical and Computer Engineering, McGill University, Montreal, QC H2W 1S6, Canada

A modified meshless local Petrov–Galerkin for an electromagnetic axisymmetric problem is presented in this paper. The method uses the shape functions generated by the radial point interpolation method with a modified T-scheme to select the support nodes, and also a new and malleable strategy to determine the test domains. The convergence of the method is evaluated using a coaxial cavity problem and it is compared with the finite-element method for two different meshes: one with a good quality mesh and another partially composed to bad quality elements. The total execution time using both methods is also compared.

***Index Terms*— Axisymmetric problems, convergence of numerical methods, meshless local Petrov–Galerkin (MLPG), meshless methods, radial point interpolation method (PIM).**

I. Introduction

SEVERAL meshless methods are reported in the literature. Among them are the element-free Galerkin [1], the meshless local Petrov–Galerkin (MLPG) [2], [3], and the point interpolation methods (PIMs) [4]–[6]. Meshless methods use a procedure to build their shape functions such as the moving least squares and the PIM [7].

In this paper, the formulation is based on the MLPG method, which has a local weak formulation, resulting in sparse matrices and minimization of the numerical effort. The radial PIM with Polynomials (RPIMp) is used to generate the shape functions. In RPIMp, radial basis functions (RBFs) and polynomials are added to the base, providing high accuracy and ensuring consistency of the shape functions [7]. RPIMp shape functions have the Kronecker delta property, and thus essential boundary conditions are naturally enforced.

The MLPG does not require any mesh or grid. However, a special data structure (generally a k-d tree) is used to determine the support and test domains [7], [8]. To improve the MLPG performance, a modified T6-scheme [7] and a new T8-scheme are used to select the support nodes, which generate the shape functions. Using mesh information to determine the test domain, the local weak form integration procedure is simplified and a better numerical precision can be obtained. Therefore, we propose an MLPG method that depends on a mesh. The advantage of the proposed method is that it is less sensitive to bad quality meshes than the FEM. To demonstrate this, the eigenvalues of a cylindrical coaxial cavity are computed for two different meshes: a good quality one and another partially composed of bad quality elements.

Manuscript received June 28, 2013; revised August 19, 2013; accepted September 24, 2013. Date of current version February 21, 2014. Corresponding author: R. D. Soares (e-mail: ramon.dornelas.soares@gmail.com).

Color versions of one or more of the figures in this paper are available online at http://ieeexplore.ieee.org.

Digital Object Identifier 10.1109/TMAG.2013.2284472

II. Mathematical Formulations

A. Global Weak Form

In this paper, an electromagnetic problem with axial symmetry is solved. A 2-D analysis (on the $\rho - z$ semiplane) is proposed, where the magnetic field only has the H_ϕ component and $\partial H_\phi/\partial\phi = 0$. Applying these assumptions in the Helmholtz vector equation, one obtains the following strong form [9]:

$$\frac{\partial}{\partial\rho}\left[\frac{1}{\rho\epsilon_r}\frac{\partial(\rho H_\phi)}{\partial\rho}\right]+\frac{\partial}{\partial z}\left[\frac{1}{\rho\epsilon_r}\frac{\partial(\rho H_\phi)}{\partial z}\right]+k^2\mu_r H_\phi = 0 \quad (1)$$

where ϵ_r and μ_r are the relative permittivity and permeability, respectively, and k is the free-space wavenumber.

Applying the weighted residual method and the divergence theorem in (1), we obtain the global weak form in the problem domain Ω [9]

$$\int_\Gamma \frac{\psi}{\rho\epsilon_r}\frac{\partial(\rho H_\phi)}{\partial n}d\Gamma - \iint_\Omega \frac{1}{\rho\epsilon_r}\nabla\psi\cdot\nabla(\rho H_\phi)d\Omega + k^2\iint_\Omega \frac{\mu_r\psi}{\rho}(\rho H_\phi)d\Omega = 0 \quad (2)$$

where Γ is the boundary of the problem domain and ψ is the test function.

B. RPIMp Approximation

Meshless methods use a set of nodes inside Ω (interior nodes) and at its boundary Γ (boundary nodes) to build approximations in a point $\mathbf{x}$ of Ω. The meshless approximation u^h can be obtained using [7]

$$u^h(\mathbf{x}) = \sum_{i\in S}\varphi_i(\mathbf{x})u_i = \Phi(\mathbf{x})\mathbf{U}_S \quad (3)$$

where S is the set of nodes in the neighborhood of point $\mathbf{x}$ (i.e., the support domain of $\mathbf{x}$), φ_i is the shape function of the ith node (built using all nodes of S), and u_i is the field variable at the ith node. Vectors Φ and $\mathbf{U}_S$ collect all the shape functions and field variables in the support domain, respectively.

In this paper, the shape functions are generated using RPIMp, combining RBFs with polynomials. An RPIMp shape function has interesting properties. It is generated by an arbitrary node distribution, which provides a description of the unknown field with a consistency defined by the polynomial terms of the base, and has the Kronecker delta property, which simplifies the treatment of essential boundary conditions [7]. Using RPIMp, u^h is given by

$$u^h(\mathbf{x}) = \sum_{i=1}^{l} R_i(\mathbf{x})a_i + \sum_{j=1}^{m} p_j(\mathbf{x})b_j = \mathbf{R}^t(\mathbf{x})\mathbf{a} + \mathbf{p}^t(\mathbf{x})\mathbf{b} \quad (4)$$

where a_i is the coefficient of the RBFs R_i, b_j is the coefficient of the monomial p_j in the polynomial base, l is the number of nodes included in the support domain of $\mathbf{x}$, and m is the number of monomials in the polynomial base. Vectors $\mathbf{R}$ and $\mathbf{p}$ collect the RBF and polynomial terms, respectively. The coefficient vectors $\mathbf{a}$ and $\mathbf{b}$ can be determined by satisfying (4) at the nodes of the support domain and imposing constraints on the polynomial basis functions to guarantee a single solution [7]

$$\mathbf{b} = \mathbf{S}_b\mathbf{U}_S, \quad \mathbf{S}_b = \left[\mathbf{P}_m^t\mathbf{R}_Q^{-1}\mathbf{P}_m\right]^{-1}\mathbf{P}_m^t\mathbf{R}_Q^{-1} \quad (5)$$

$$\mathbf{a} = \mathbf{S}_a\mathbf{U}_S, \quad \mathbf{S}_a = \mathbf{R}_Q^{-1} - \mathbf{R}_Q^{-1}\mathbf{P}_m\mathbf{S}_b \quad (6)$$

where $\mathbf{R}_Q$ and $\mathbf{P}_m$ are the moment matrices associated with $\mathbf{R}(\mathbf{x})$ and $\mathbf{p}(\mathbf{x})$, respectively, both evaluated at all l nodes.

From (4)–(6), the shape functions and their derivatives with respect to normal direction $\hat{n}$ in the semiplane $\rho - z$ are, respectively, given by

$$\Phi(\mathbf{x}) = \mathbf{R}^t(\mathbf{x})\mathbf{S}_a + \mathbf{p}^t(\mathbf{x})\mathbf{S}_b \quad (7)$$

$$\hat{n}\cdot\nabla\Phi(\mathbf{x}) = \frac{\partial\Phi(\mathbf{x})}{\partial n} = \frac{\partial\mathbf{R}^t(\mathbf{x})}{\partial n}\mathbf{S}_a + \frac{\partial\mathbf{p}^t(\mathbf{x})}{\partial n}\mathbf{S}_b. \quad (8)$$

III. Modified MLPG

The MLPG solution of (2) is achieved by approximating ρH_ϕ by u^h of (4). The RPIMp shape functions are built using a modified T-scheme for node selection in the support domain. T-schemes are based on background triangular cells and ensure more efficiency in the computation of the shape functions [8]. There are two kinds of T-schemes: a cell-based and an edge-based T-scheme, for $\mathbf{x}$ located inside or at the edge of a triangular cell, respectively [8].

For the cell-based scheme, a modified T6-scheme is adopted. If the triangular cell is in the interior of Ω, the usual T6-scheme is applied with the six nodes given by the three triangle vertices plus the opposite vertices of the three neighboring triangles. If the triangular cell is at the boundary of Ω, then only five nodes are specified as there are two neighboring triangles. For the new edge-based T-scheme, the nodes are defined by the four vertices of the triangles, which share the corresponding edge plus the opposite vertices of the neighboring triangles around, as shown in Fig. 1(a). When the edge is located on an element at the boundary, fewer nodes are selected, as shown in Fig. 1(b), where six nodes were selected. Both cell and edge-based schemes do not use a search structure to add a node to boundary cells, which is simpler and more

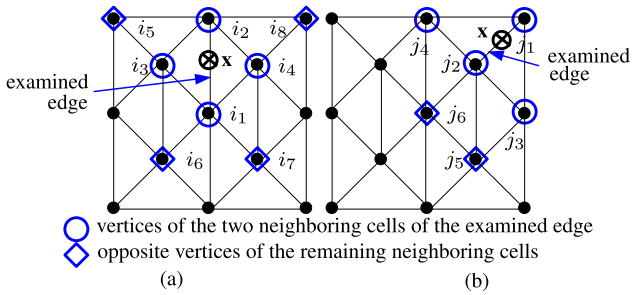

Fig. 1. Proposed edge-based T-scheme with (a) eight nodes and (b) six nodes.

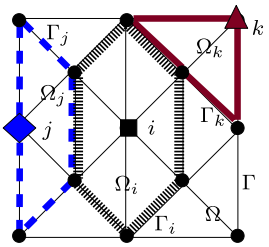

Fig. 2. Test domains of nodes i, j, and k.

efficient when compared with standard T-schemes, and also provide fast convergence, as will be shown in Section IV.

For a given node i, its test function ψ_i has a compact support where $\psi_i \neq 0$, which defines the node's test domain Ω_i where weak-form integrations are evaluated. We propose to use the mesh to determine Ω_i, which is composed of all triangular cells that have the node i as one of its vertices. Fig. 2 shows three test domains (Ω_i, Ω_j, and Ω_k) and their boundaries (Γ_i, Γ_j, and Γ_k) for three different node locations (i, j, and k). The adopted test function is a Heaviside step, which has a unit value inside the corresponding test domain and its boundary. The use of a Heaviside step function provides solutions with accuracy and fast convergence [10].

The MLPG local weak form is then obtained from (2) by replacing ψ by 1 and ρH_ϕ by its RPIMp approximation (4). In (2), the second integral vanishes, as $\nabla\psi = 0$ inside the test domain Ω_i. The boundary integral of (2) is evaluated only for Γ_i inside Ω. For Γ_i on Γ, assumed to be a perfect electric conductor wall, the boundary integral is used to impose the Neumann boundary condition $\partial(\rho H_\phi)/\partial n = 0$. Applying those assumptions in (2), one obtains the following system:

$$k^2\mathbf{C} + \mathbf{D} = 0 \quad (9)$$

where

$$\mathbf{C}_{ij} = \iint_{\Omega_i} \frac{\mu_r\varphi_j}{\rho}d\Omega \quad \text{and} \quad \mathbf{D}_{ij} = \int_{\Gamma_i} \frac{1}{\rho\epsilon_r}\frac{\partial\varphi_j}{\partial n}d\Gamma.$$

IV. Numerical Results

Numerical results are presented for the resonant modes of an axially symmetric coaxial cavity [11]. The analyzed cavity has an internal radius of 1 m, an external radius of 2 m, a height equals to 1 m, and vacuum in its interior ($\epsilon_r = 1$ and $\mu_r = 1$). Only the first five modes with $E_\phi = 0$ and $\partial H_\phi/\partial\phi = 0$ are considered. MLPG convergence is determined and compared

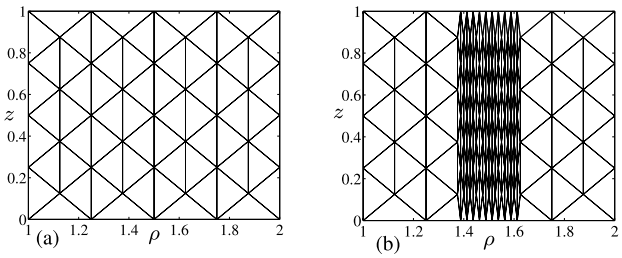

Fig. 3. Used meshes. (a) Mesh A with high-quality elements, 41 nodes. (b) Mesh B partially built with bad quality elements, 122 nodes.

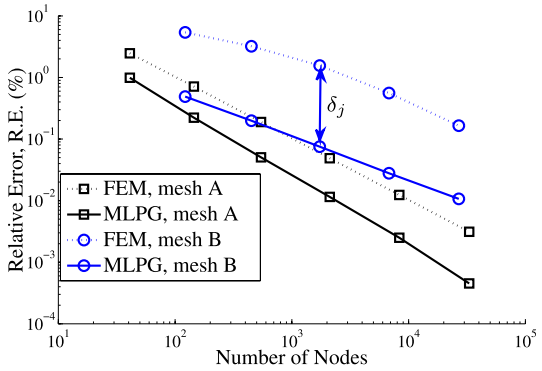

Fig. 4. MLPG and FEM convergence using meshes A and B for the second mode of the coaxial cavity as a function of the number of nodes.

with FEM. The convergence for both methods is determined by the relative error as a function of the maximum spacing between the nodes of each mesh. The relative error given for each mesh is determined by

$$\text{R.E.} = \frac{|k_y^{\text{Num}} - k_y^{\text{Exact}}|}{k_y^{\text{Exact}}} \cdot 100\% \tag{10}$$

where k_y^{Num} and k_y^{Exact} are the numerical and exact solutions of the yth eigenvalue (i.e., $k_y = \omega_y\sqrt{\mu_0\epsilon_0}$ and ω_y is the resonance frequency of the yth mode of the cavity).

Two different meshes are used: the first one (mesh A) has only high-quality elements [Fig. 3(a)] and the second one (mesh B) is partially built with bad quality elements with one internal angle close to 180° [Fig. 3(b)]. Fig. 4 shows the convergence for the second mode k_2 of the coaxial cavity. The MLPG convergence results are better than the FEM results for both meshes. The MLPG convergence rates (i.e., measure of how fast the numerical results converge to the analytical solution when space between nodes decreases) are 2.2015 and 1.3876 and the FEM ones are 1.9327 and 1.2595 for meshes A and B, respectively. Fig. 4 also shows the parameter δ_j that defines the logarithmic level difference between FEM and MLPG errors at each point j of the curves. The average logarithmic level difference δ_{av} is computed using all δ_j with the same number of mesh nodes. In Fig. 4, $\delta_{\text{av}} = 0.6062$ and $\delta_{\text{av}} = 1.2118$ for meshes A and B, respectively. From Fig. 4, one observes that δ_{av} increases from mesh A to B, suggesting a lower sensitivity of the MLPG to mesh distortion.

The convergence rates of the eigenvalues for the first five modes are shown in Table I, which presents the results for FEM using meshes A and B (FEM-A and FEM-B) and for MLPG using the same meshes (MLPG-A and MLPG-B). For the regular mesh A, MLPG has higher convergence rates than FEM for modes k_2, k_3, and k_5, and FEM has better results for k_1 and k_4. The convergence rates are quite similar, showing that FEM and MLPG have similar performance for the regular mesh A. However, regarding the bad quality mesh B, MLPG has higher convergence rates than FEM for modes k_1, k_2, k_3, and k_5 while FEM has a slightly larger rate only for mode k_4, showing that MLPG generally achieves better performances than FEM for this mesh.

TABLE I
MLPG AND FEM CONVERGENCE RATES

Modes	k_1	k_2	k_3	k_4	k_5
FEM-A	2.0928	1.9327	1.9809	2.0924	1.9347
MLPG-A	1.9477	2.2015	1.9848	2.054	2.0869
FEM-B	2.1059	1.2595	1.7622	2.0835	1.1982
MLPG-B	2.4599	1.3876	1.8058	2.0339	1.5765

TABLE II
AVERAGE LOGARITHMIC LEVEL DIFFERENCE

Modes	k_1	k_2	k_3	k_4	k_5
δ_{av}-A	-0.1571	0.6062	0.0789	-0.1937	0.5741
δ_{av}-B	0.4663	1.2118	0.4389	-0.2827	1.3432

TABLE III
TOTAL TIME TO SOLVE THE PROBLEM (SECONDS) × NUMBER OF NODES

Meshes A	A_1	A_2	A_3	A_4	A_5	A_6
Nodes	41	145	545	2113	8221	33025
FEM time	0.07	0.24	0.85	3.42	15.05	77.39
MLPG time	0.30	1.1	4.35	17.8	75.42	345.26

Meshes B	B_1	B_2	B_3	B_4	B_5
Nodes	122	451	1733	6793	26897
FEM time	0.18	0.68	2.57	11.31	56.12
MLPG time	0.90	3.57	14.60	60.57	269.88

The average logarithmic level difference for MLPG and FEM error curves is shown in Table II for the first five modes of the cavity. δ_{av} are presented for the two meshes A and B (δ_{av}-A and δ_{av}-B). For mesh A, the MLPG has better results for the modes k_2, k_3, and k_5, which are below the FEM error curves by 0.6062, 0.0789, and 0.5741, respectively. FEM has better results for modes k_1 and k_4, which are below the MLPG curves by 0.1571 and 0.1937, respectively. For mesh B, MLPG does not provide better results only for mode k_4. This may be related to the field distribution of that particular mode, which is the TM mode with $n = q = 0$ and $p = 3$ according to [11, Ch. 5]. This mode does not vary with z and has a small variation with ρ for $\rho \approx 1.5$, in which case mesh B may not be as bad as it is for the other four modes.

The MLPG time to solve a problem is always bigger than FEM for the same mesh, as shown in Table III. However, a fairer comparison between the methods can be done using the obtained error as a function of the computational time.

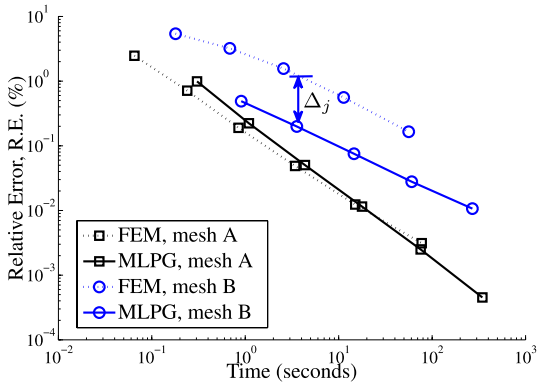

Fig. 5. MLPG and FEM convergence using meshes A and B for the second mode of the coaxial cavity with respect to time.

TABLE IV
AVERAGE LOGARITHMIC LEVEL DIFFERENCE WITH RESPECT TO TIME

Modes	k_1	k_2	k_3	k_4	k_5
Δ_{av}-A	-0.7858	-0.0341	-0.5341	-0.8321	-0.039
Δ_{av}-B	-0.3518	0.8329	-0.1235	-0.9407	0.9106

This is shown in Fig. 5 for the second mode (k_2) and for both meshes, A and B. These results were obtained using a personal computer (Intel Core i7, quad core processor at 2 GHz). The better performance of MLPG over FEM is evident in this figure for the mesh B. For mesh A, the performances of both methods are very similar.

Convergence comparisons for modes k_1, k_3, k_4, and k_5 are conducted using a new parameter Δ_j, which shows the logarithmic level error difference between MLPG-B$_j$ and a point in the FEM-B curve obtained by a linear interpolation (see Fig. 5). Δ_j is used to compute the average logarithmic level difference Δ_{av}-A and Δ_{av}-B, which are shown in the Table IV for modes $k_1 - k_5$. For mesh A, the FEM has better results with respect to time for modes k_1, k_3, and k_4, which are below the MLPG error curves by 0.7858, 0.5341, and 0.8321, respectively. MLPG and FEM have close results for the modes k_2 and k_5, but here also the FEM results are below the MLPG curves by 0.0341 and 0.039, respectively. For mesh B, MLPG does not provide a better result for modes k_1 and k_4. For mode k_3, close results between both methods are found and MLPG shows better results for modes k_2 and k_5. The Δ_{av} results provide evidence for the similar performance with respect to time between the proposed MLPG and FEM using mesh B.

V. CONCLUSION

In this paper, new edge-based and modified cell-based T schemes have been proposed to determine the support domains of the MLPG numerical simulations. They are simpler and more efficient when compared with the standard ones, and also provide high convergence rates. A new strategy to determine the test domains was presented, which is more easily adaptable to the problem geometry.

The proposed MLPG was used to calculate the eigenvalues of an axisymmetric cavity. The numerical results suggest a better performance of the proposed MLPG than FEM in problems with meshes with badly shaped elements, in which MLPG generally presents better convergence rates for most of the cavity modes. The results also suggest that the accuracy of the proposed method and FEM depends on the field distribution of the analyzed mode, the mesh shape and position of the bad elements, but further work has to be done to explain the reasons for this.

The MLPG spent more time to solve the problems than FEM, but its errors, using the same mesh, were smaller than those of FEM for most of the cavity modes analyzed. When time and error measures were simultaneously considered, FEM showed better performances than MLPG for good-quality meshes and both methods showed similar performances for bad-quality ones. These results encourage the application of the proposed MLPG in 3-D problems, where badly shaped meshes may frequently occur.

ACKNOWLEDGMENT

This work was supported in part by "Numerical Investigation of Coupled Electromagnetic Field Problems," UFMG (Brazil) and McGill University (Canada), CAPES-DFAIT, in part by CNPQ, and in part by FAPEMIG.

REFERENCES

[1] E. H. R. Coppoli, R. C. Mesquita, and R. S. Silva, "Induction machines modeling with meshless methods," *IEEE Trans. Magn.*, vol. 48, no. 2, pp. 847–850, Feb. 2012.

[2] W. Nicomendes, R. Mesquita, and F. Moreira, "Calculating the band structure of photonic crystals through the meshless local Petrov-Galerkin (MLPG) method and periodic shape functions," *IEEE Trans. Magn.*, vol. 48, no. 2, pp. 551–554, Feb. 2012.

[3] B. C. Correa, E. J. Silva, A. R. Fonseca, D. B. Oliveira, and R. C. Mesquita, "Meshless local Petrov-Galerkin approach in solving microwave guide problems," *IEEE Trans. Magn.*, vol. 47, no. 5, pp. 1526–1529, May 2011.

[4] N. Z. Lima, A. R. Fonseca, and R. C. Mesquita, "Application of local point interpolation method to electromagnetic problems with material discontinuities using a new visibility criterion," *IEEE Trans. Magn.*, vol. 48, no. 2, pp. 615–618, Feb. 2012.

[5] N. Z. Lima, R. C. Mesquita, W. G. Facco, A. S. Moura, and E. J. Silva, "The nonconforming point interpolation method applied to electromagnetic problems," *IEEE Trans. Magn.*, vol. 48, no. 2, pp. 619–622, Feb. 2012.

[6] D. Soares, "Time-domain electromagnetic wave propagation analysis by edge-based smoothed point interpolation methods," *J. Comput. Phys.*, vol. 234, pp. 472–486, Feb. 2013.

[7] G. R. Liu, *Mesh Free Methods: Moving Beyond the Finite Element Method*, 2nd ed., Cleveland, OH, USA: CRC Press, 2009.

[8] G. R. Liu and G. Y. Zhang, "A normed G space and weakened weak (W^2) formulation of a cell-based smoothed point interpolation method," *Int. J. Comput. Methods*, vol. 6, no. 11, pp. 147–179, 2009.

[9] A. Peterson, S. Ray, and R. Mittra, *Computational Methods for Electromagnetics*. Piscataway, NJ, USA: IEEE Press, 1998, pp. 3–332.

[10] S. N. Atluri and S. Shen, "The meshless local Petrov-Galerkin (MLPG) method—A simple and less-costly alternative to the finite element and boundary element methods," *CMES—Comput. Model. Eng. Sci.*, vol. 3, no. 1, pp. 11–51, 2002.

[11] R. F. Harrington, *Time Harmonic Eletromagnetic Field*. New York, NY, USA: Wiley, 2001, pp. 198–256.